JOURNAL OF CATALYSIS 151, 439–452 (1994)

Oxidative Coupling of Methane over Lanthana Catalysts

I. Identification and Role of Specific Active Sites

S. Lacombe, C. Geantet, and C. Mirodatos

Institut de Recherches sur la Catalyse, 2 Avenue Albert Einstein, 69626 Villeurbanne Cedex, France

Received April 19, 1994; revised September 1, 1994

The present work aims at coorelating the surface characteristics of a "working" catalyst under the conditions of the oxidative coupling of methane (OCM) with mechanistic aspects of the reaction deduced from transient experiments focused on the total oxidation pathway. Several lanthana samples with variable surface area and morphology are tested with a view to identifying the exact nature of OCM-specific active sites. The lanthana surface, characterized by XPS, TEM, XRD, FTIR, and *in situ* DRIFT spectroscopy, appears to be mostly decarbonated and dehydroxylated under reaction conditions. Low coordination sites localized on step edges are related to the total oxidation pathway, while basic sites associated with oxygen vacancies enable the oxygen activation leading to the initial methane activation. Structure sensitivity effects are explained within this proposal of differentiated sites on a typical OCM catalyst. © 1995 Academic Press, Inc.

INTRODUCTION

Since the pioneering works of Keller and Bhasin (1), numerous advances have been made in the study of the oxidative coupling of methane (OCM) over basic oxides. Nevertheless, several points regarding the fundamentals of the reaction still remain to be elucidated, among them the nature of the active sites both for coupling and for the total oxidation of methane. Although the formation of methyl radicals from methane has been convincingly established by various methods (2–4), the initial activation step is still controversial (2, 5). Concerning the deep oxidation of methane into CO and CO_2, generally lumped together as CO_x, there is still debate about the related active sites and mechanistic pathway(s). Shi *et al.* (6) proposed that CO and CO_2 come from a gas-phase chain-branching oxidation process involving the reaction of methyl radicals with gaseous oxyen. By comparing the ratios CO/CO_x obtained either from CH_4 or from CD_4 on NaOH/CaO catalysts, Lehmann and Baerns (7) concluded that CO and CO_2 formation present the same rate-determining step, which is the formation of formaldehyde from the reaction of methyl radicals with surface basic oxygen. Lacombe *et al.* (8) proposed that on lanthana catalysts CO_2 is formed on the catalyst surface, involving a slow step of methyl radical oxidation, while CO issues from the C_2's. The proposal is in good keeping with the observation of distinct kinetic isotopic effects on CO (a value close to the KIE value observed for the C_2's formation) and on CO_2 (almost negligible).

An effective way to specify the nature of the active sites in a complex reaction is to compare the configuration of the working surface determined from *in situ* catalyst characterization with the actual concentration of active sites determined from steady-state isotopic transient kinetics (SSITK) (9). This procedure, which has been successfully applied to catalysis on metals, is more delicate for the case of oxidative catalysis due to (i) the instability of the oxide phases and/or the formation of new phases under catalytic reaction conditions, which complicates the characterization of the working surface, and (ii) the presence of short-lived adsorbed species which may require transient techniques with a shorter time resolution such as the pulsed temporal resolution of products (TAP) reactor (4, 10, 11).

The present work aims at correlating the surface characteristics of a "working" catalyst with mechanistic aspects of the reaction deduced from transient experiments focused on the total oxidation pathway. The chosen catalyst is nonpromoted lanthanum oxide, often used as a major constituent of patented OCM formulas. It is active and rather stable, though its phase composition is known to be highly dependent on preparation and activation methods. In terms of structural stability, lanthanum oxide is very sensitive to water and carbon dioxide in the surrounding atmosphere (12). Since the reaction of oxidative coupling of methane produces significant amounts of water and carbon dioxide, the state of the catalyst is therefore likely to be deeply modified under reaction conditions. Taylor and Schrader (13) observed that whatever the starting bulk material—La_2O_3, $La(OH)_3$, $La_2O_2CO_3$, or $La_2(CO_3)_3$—the final bulk phase after treatment under

0021-9517/95 $6.00

OCM conditions at 750°C was mostly, if not only, La_2O_3. Nevertheless, catalytic performance was found to depend on the nature of the starting material. It may be related to differences in surface composition (which indeed may differ from bulk composition) and/or in morphology, since the starting materials went through important changes during the steps of catalyst activation and start-up. Le Van *et al.* (14) have indeed emphasized the market effect of morphology on the catalytic behaviour of lanthana materials. In order to specify this obvious relationship between morphology and catalytic performance, several lanthana samples with variable surface area and morphology were tested within the above scope of identifying the exact nature of OCM-specific active sites.

EXPERIMENTAL

Catalyst Preparation

A series of lanthanum oxide catalysts was prepared from lanthanum nitrate $La(NO_3)_3 \cdot 6\ H_2O$ supplied by Rhône–Poulenc by the following procedure: (i) decomposition of the nitrate under air at 500°C for 3 h (involving a step of liquefaction), (ii) crushing of the powder and sieving to 200–300 μm, (iii) calcination under pure oxygen at variable temperature for 2 h (flow rate of 0.5 cm^3/s). A supplementary catalyst presenting a larger surface area, La_{LS}, was supplied by Rhône–Poulenc. The lanthanum oxide samples were characterized either after calcination (between 650 and 1000°C) or after OCM reaction at 750°C as further specified. In each characterization procedure care was taken to minimize, if not eliminate, any contact with the open air.

Surface Area

Sample surface areas were measured on an automated nitrogen adsorption volumetric apparatus, according to the BET method. A special cell was used allowing both the dynamic catalyst activation and the static BET measurements, without transfer in the open air. Samples were outgassed at 450°C for 2 h before nitrogen adsorption.

X-Ray Diffraction

Samples were analyzed on a Philips PW1710 diffractometer, equipped with a Cu anode. The activated samples were transferred from the catalytic reactor to the XRD chamber under dried nitrogen, except during the grid preparation. The surrounding atmosphere was kept free from water.

Electron Microscopy

Transmission electron microscopy (TEM) was carried out on a JEOL 2010 microscope. The sample was deposited as a dry powder on a thin carbon film mounted on a copper grid.

X-Ray Photoelectron Spectroscopy

XPS measurements were carried out on a VG-type ESCA III spectrometer (photon energy 1486.6 eV, Al$K\alpha$). The samples were treated directly on the sample holder in a heated reaction chamber under flowing gases (either pure oxyen for calcination or $CH_4/O_2/He$ mixture for OCM reaction), then purged under helium, cooled, evacuated, and transferred into the XPS chamber. The raw XPS spectra were smoothed and corrected for the background. The binding energies were calibrated with respect to the C_{1s} energy at 284.5 eV corresponding to the adventitious carbon. The atomic ratios betweeen the different elements (La, O, and C) were calculated, accounting for their cross section and mean free path (15).

Transmission Fourier Transform IR Spectroscopy

Transmission FTIR analyses were performed on a Brücker IFS 110 spectrometer. The same cell was used for catalyst treatment and IR analysis. The sample, prepared as a thin wafer of 50 mg, was analyzed at room temperature (i) after calcination at 750°C under flowing oxygen, (ii) after reaction at 750°C for 2 h under a flowing $CH_4/O_2/He$ mixture, and (iii) after 1 h evacuation at increasing temperature, a spectrum being recorded after each desorption step.

In Situ Diffuse Reflectance Fourier Transform Infrared Spectroscopy

Additional FTIR experiments were carried out with a Spectra-Tech diffuse reflectance infrared cell (1.5 cm^3 of inner volume), adapted to a Nicolet 550 spectrometer. The cell was connected to the catalytic testing set-up, so that gas mixtures could flow through the catalyst bed as for a conventional dynamic microreactor, to be further analyzed by GC and MS; it allowed *in situ* treatments at high temperatures (up to around 800°C) and under controlled atmosphere (O_2/He and $CH_4/O_2/He$ flowing mixtures). About 50 mg of untreated lanthana powder was loaded into the DRIFT cell, then heated to 750°C under a flowing O_2/He mixture and finally contacted with the $CH_4/O_2/He$ mixture. DRIFT spectra were recorded regularly (around 30 s acquisition per spectrum) in order to observe the changes in the DRIFT pattern when temperature and gas composition were changed. The DRIFT spectra were converted into Kubelka–Munk units.

Steady-State Isotopic Transient Kinetics (SSITK)

The isotopic transient experiments under steady state aim at measuring the residence time of the reactants and

products in the catalytic system (9). They were carried out by abrupt switching with an automated four-way valve located just before the reactor, from the nonlabelled feeding mixture $^{12}CH_4/^{16}O_2$/He (8/4/88, 0.5 cm^3/s) to either the $^{13}CH_4/^{16}O_2$/He- or the $^{12}CH_4/^{18}O_2$/He-labelled mixture with the same flow rate and composition. The total concentration of each gas was analyzed at the reactor outlet by on-line gas chromatography. The isotopic distribution of each gas was continuously monitored during the transients by on-line mass spectrometry (amu 15, 17, 44, 45 for $^{12}CH_4$, $^{13}CH_4$, $^{12}CO_2$, and $^{13}CO_2$, respectively). Due to mass overlapping, carbon monoxide, ethane, and ethylene were analyzed by GC–MS coupling by using a 12-loop valve for sampling the gases during the isotopic transient.

The overall residence time of a reaction product measured by SSITK actually includes (i) the catalytic time due to the proper transformation of the reactant into the product on a catalytic site and (ii) the so-called chromatographic effect due to readsorption/desorption equilibria of the product along the catalytic bed and in the gas line. The chromatographic effect occurring along the catalyst bed was corrected for by measuring the overall residence time with different catalyst loadings and extrapolating to zero loading. Concerning the chromatographic effect along the gas line, two prereactors were added to the set-up; each of them contained the same amount of lanthanum oxide and was fed with either a nonlabelled reacting mixture ($^{12}CH_4/O_2$/He) or a carbon-labelled reacting mixture ($^{13}CH_4/O_2$/He). The proper reactor was filled with quartz. Switching the two lines at the reactor inlet thus enabled one to follow the transient behaviour of the labelled/nonlabelled mixtures of the products and to measure their retention time in the system excluding their formation time (9).

RESULTS

Catalyst Characterization

Surface area. The BET surface areas measured after calcination at different temperatures and after OCM reaction are reported in Table 1. For the ex-nitrate samples the decrease in surface area observed when the calcination temperature was increased indicates that lanthanum oxide sintering occurs in the 650–1000°C temperature range starting from the initial hydroxide material. No further effect on surface area was observed after OCM reaction at 750°C, except for the sample calcined at 650°C and for the large surface La_{LS} sample.

Crystalline structure. After calcination at 650°C or after reaction at 750°C, all samples were identified as lanthanum oxide with a hexagonal structure, as revealed by XRD analysis (Figs. 1a and b, respectively); however a few percent of hydroxide was still detected after calcination at 650°C (Fig. 1a). The absence of other bulk phases such as lanthanum carbonates, even after reaction, was consistent with the observations of Taylor and Schrader (13). It should be mentioned, however, in line with the recent work of Squire *et al.* (16) carried out by *in situ* XRD, that slight amounts of bulk oxycarbonate could exist under the reaction conditions, not observable by *ex situ* XRD since they decompose at room temperature. A freshly prepared and activated lanthanum oxide sample left in the open air (Fig. 1c) turned out to be completely hydrated into $La(OH)_3$, which confirms the high sensitivity of lanthanum oxide to the surrounding atmosphere. No specific crystallographic orientation could be deduced from the XRD patterns. The peak width, close to the limits fixed by the diffractometer, corresponded to a minimum particle size of 100 nm.

TABLE 1

Change in Surface Area as a Function of the Calcination Temperature and after OCM Reaction

Sample	Precursor	Calcination Temperature (°C)	Surface area (m^2/g, ±0.2) After calcination	Surface area (m^2/g, ±0.2) After reaction at 750°C
La_{LS}	Unknown	800	11.0	4.5
La_{650}	$La(NO_3)_3$, $6H_2O$	650	3.3	2.4
La_{750}	$La(NO_3)_3$, $6H_2O$	750	2.4	2.4
La_{1000}	$La(NO_3)_3$, $6H_2O$	1000	1.0	1.0

Surface composition by ex situ transmission infrared spectroscopy. An *ex situ* infrared spectroscopy study

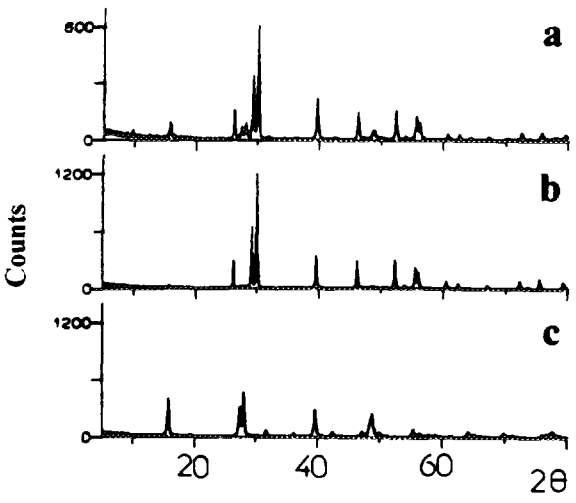

FIG. 1. XRD patterns (corrected for background) of a La_2O_3 sample recorded after the indicated consecutive treatments: (a) calcination at 650°C; (b) reaction at 750°C; (c) sample calcined at 650°C and left in the open air.

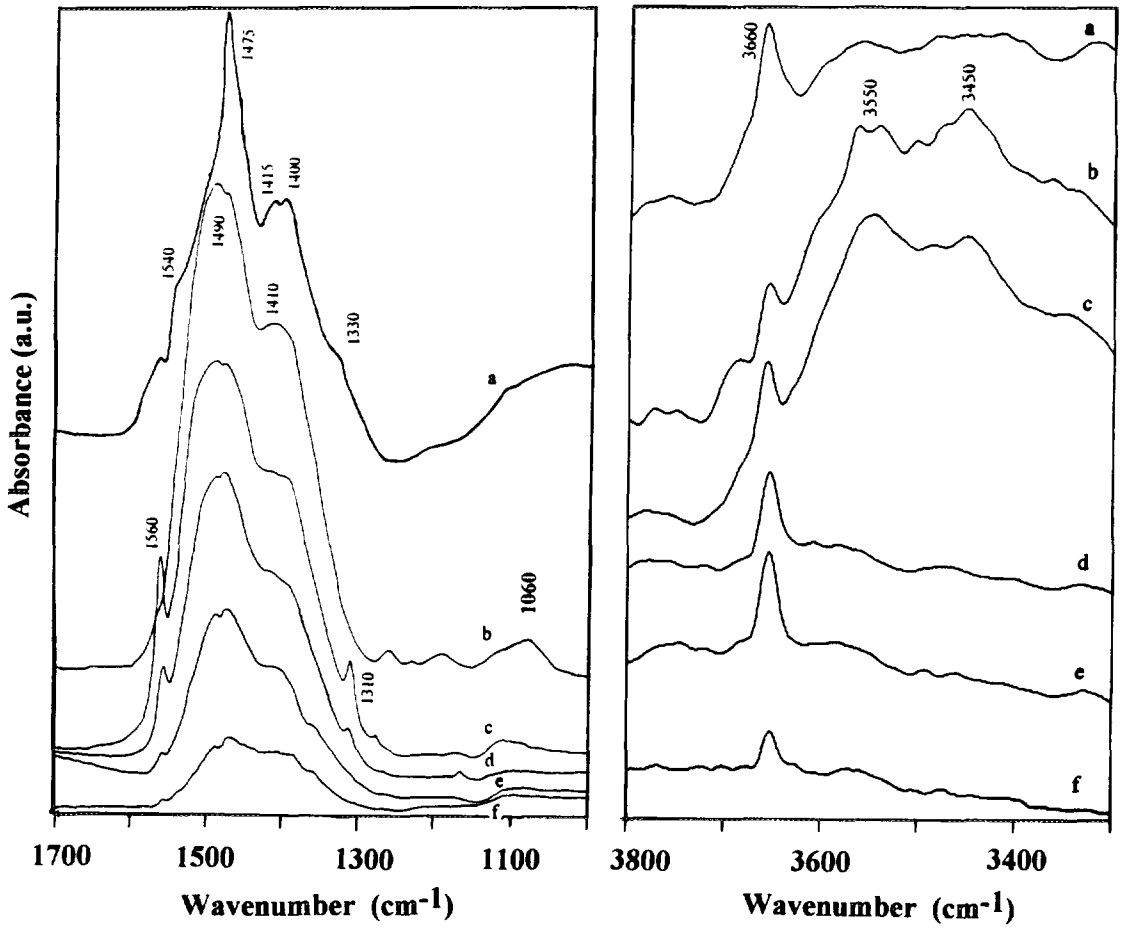

FIG. 2. Infrared spectra ranges, recorded at room temperature in the transmission mode after the indicated consecutive treatments: (a) calcination at 750°C for 2 h; (b) reaction at 750°C for 2 h; (c) 1 h evacuation at 25°C; (d) 1 h evacuation at 350°C; (e) 1 h evacuation at 500°C; (f) 1 h evacuation at 700°C.

was carried out on the La_{750} sample in order to identify the surface composition and the changes induced by the reaction. The transmission infrared spectra, recorded at room temperature, are reported in Fig. 2.

After calcination at 750°C (Fig. 2a), infrared absorption is observed (i) in the range 3700–3200 cm^{-1}, with a sharp band at 3660 cm^{-1} superimposed on a broad absorption formed of several badly resolved peaks between 3550 and 3200 cm^{-1}, and (ii) in the range 1600–1300 cm^{-1} with several peaks and shoulders at 1540, 1490, 1475, 1415, 1400, 1330 cm^{-1}. Of the high frequency range (hydroxyl groups), the band at 3660 cm^{-1} cannot be assigned to the O–H stretching vibration of bulk lanthanum trihydroxide $La(OH)_3$ since the latter absorbs at 3590 and 3610 cm^{-1} and should decompose at around 300°C (17). It probably corresponds to isolated surface terminal La–OH groups, by analogy with the weakly acidic species observed on silica or on alumina (18). By contrast, the broad absorption between 3550 and 3200 cm^{-1} may be assigned to interacting OH groups. The group of low frequency bands (1600–1300 cm^{-1}) corresponds to the usual vibration range of carbonate species (13, 17, 19). More precisely, according to the work of Rosynek and Magnuson (17) and of Turcotte *et al.* (19) on rare-earth oxide carbonates, the bands at 1490 and 1415 cm^{-1} can be assigned to surface monodentate carbonate derived from the reaction of CO_2 with basic surface oxygen atoms; the bands at 1540, 1475, 1400, and 1330 cm^{-1} would reflect rather the presence of carbonate species close to the dioxomonocarbonate $La_2O_2CO_3$ of type IA (distorted monoclinic structure).

After OCM reaction, the spectrum recorded under the reacting atmosphere (Fig. 2b) reveals the following changes: (i) the hydroxyl band at 3660 cm^{-1} is significantly decreased (43% of the initial band intensity), while large bands develop at 3450 and 3550 cm^{-1}; and (ii) carbonate bands are significantly enhanced, mainly at 1490 and 1415 cm^{-1} (monodentate surface carbonate).

After evacuation at room temperature (Fig. 2c), the 3660

cm^{-1} band is partially restored (68% of the initial band intensity). After evacuation at higher temperature (Fig. 2d), the low frequency OH bands (3450–3550 cm^{-1}) disappear rapidly while the 3660 cm^{-1} band is restored to its initial intensity and remains stable up to around 300°C; at higher temperature (Figs. 2e and 2f) it decreases progressively to be almost eliminated after evacuation at 800°C. In the meantime, the carbonate bands decrease continuously with transient formation of new small bands at 1310 and 1560 cm^{-1}; the latter may be assigned to bidentate carbonate entities generated by rearrangement of unidentate species as the surface coverage decreases (17). After evacuation at 800°C only traces of carbonate bands are still visible.

From the disappearance of most of the low frequency hydroxyl groups and carbonates after evacuation at 700–800°C, it may be deduced that these species observed at room temperature either after calcination or after OCM reaction are mostly due to water and carbon dioxide produced during the high temperature treatments and trapped on the catalyst when the sample was cooled. It can be inferred that under reaction conditions (750°C) the catalyst is mostly present as lanthanum oxide, possibly including traces of oxycarbonate, in accordance with the XRD analysis reported above. Similar conclusions were also reached by Le Van *et al.* (20), who emphasized recently that the amount of carbon dioxide present in the gas phase during the reaction at 650–750°C was not sufficient to convert the oxide into oxycarbonate to any large extent.

The high frequency hydroxyl groups at 3660 cm^{-1} are significantly weakened after OCM reaction (i.e., in the presence of methane and oxygen) and progressively restored after evacuation under vacuum at increasing temperature. Any direct interaction with oxygen can be discarded since this band is important even in the presence of pure oxygen, i.e., after calcination. Therefore it can be speculated that the terminal OH groups react with gaseous methane. From the IR spectra no significant accumulation of surface carbon species was visible. On the other hand, methoxide ions, $MOCH_3$, have been proposed as possible intermediate species in the surface oxidation path leading to CO_x products (7, 21, 22, 23). This was supported by the indirect observation of different H/D kinetic effects on C_2 and CO_x pathways, inducing different rate-determining steps. Direct evidence for methoxy species was provided by Tong and Lunsford (23), who reacted at room temperature reducible rare-earth oxides such as ceria with $CH_3\cdot$ radicals produced by a radical generator device. Methoxide ions are assumed to present IR bands between 2960 and 2800 cm^{-1} for C–H vibrations and between 1100 and 1060 cm^{-1} for C–O vibrations (13, 15, 23). In the present IR spectrum recorded under the reacting mixture after OCM reaction, the IR absorption of gaseous methane prevented any observation of methoxide bands in the 2800–3200 cm^{-1} range; however, a weak band was observed at 1060 cm^{-1} (Fig. 2b), which disappeared after evacuation at increasing temperature (Figs. 2d–2f). It is therefore tentatively proposed to correlate the partial disappearance of the high frequency La–OH groups after OCM reaction to the formation of La–O–CH_3 species; the latter would be trapped on the catalyst at room temperature under the reacting mixture and removed upon evacuation. Actually, the high frequency La–OH groups would be decomposed into reactive surface sites at reaction temperature, able to react with methane or with activated intermediates such as methyl radicals to form methoxide ions. Equations [1] and [2] anticipate a plausible pathway for that process, which will be strengthened further by

$$2(OH^-) \rightarrow (O^{2-}) + \square + H_2O \qquad [1]$$

$$CH_3 + (O^{2-}) + \square \rightarrow (CH_3O^-) + \boxdot, \qquad [2]$$

where species in parentheses are surface species, $\square$ is an oxygen vacancy, and $\boxdot$ is a vacancy associated with one electron.

To summarize the above IR study, it is suggested that surface intermediates such as methoxide ions M–O–CH_3 are formed on the lanthanum oxide catalysts in the course of the OCM reaction. The formation of these species would be related to the dehydroxylation of terminal La–OH groups leading to the formation of a complex site {O^{2-}, vacancy}; this site would allow the adsorption of a methyl radical colliding with the surface. Once stabilized, the La–O–CH_3 species would undergo a further oxidation, as will be specified later. Thus, specific hydroxyl groups from the lanthana surface could act as methyl radical scavengers.

Surface composition by in situ diffuse reflectance infrared spectroscopy. At variance with the previous study carried out *ex situ* in the transmission mode, the diffuse reflectance cell allowed a true *in situ* analysis, combining reaction and surface characterization. Under these conditions the problems of carbon dioxide and water trapping during the IR analysis were avoided. The diffuse reflectance spectra obtained with the La_{750} sample are reported in Figs. 3 and 4.

The changes in surface composition from the initial state of the catalyst at room temperature to the activated state at 750°C under flowing oxygen are illustrated in Fig. 3 for the hydroxyl and carbonate absorption ranges. In its initial state (i.e., before any thermal treatment), the catalyst mainly presents strong IR absorption at 3610 and 3450 cm^{-1}, and very little absorption in the carbonate range. This spectrum can be assigned to hydrated bulk $La(OH)_3$, containing only traces of carbonates, *in* accordance with the XRD data obtained with a lanthanum oxide kept in the open air (12). When the calcination tempera-

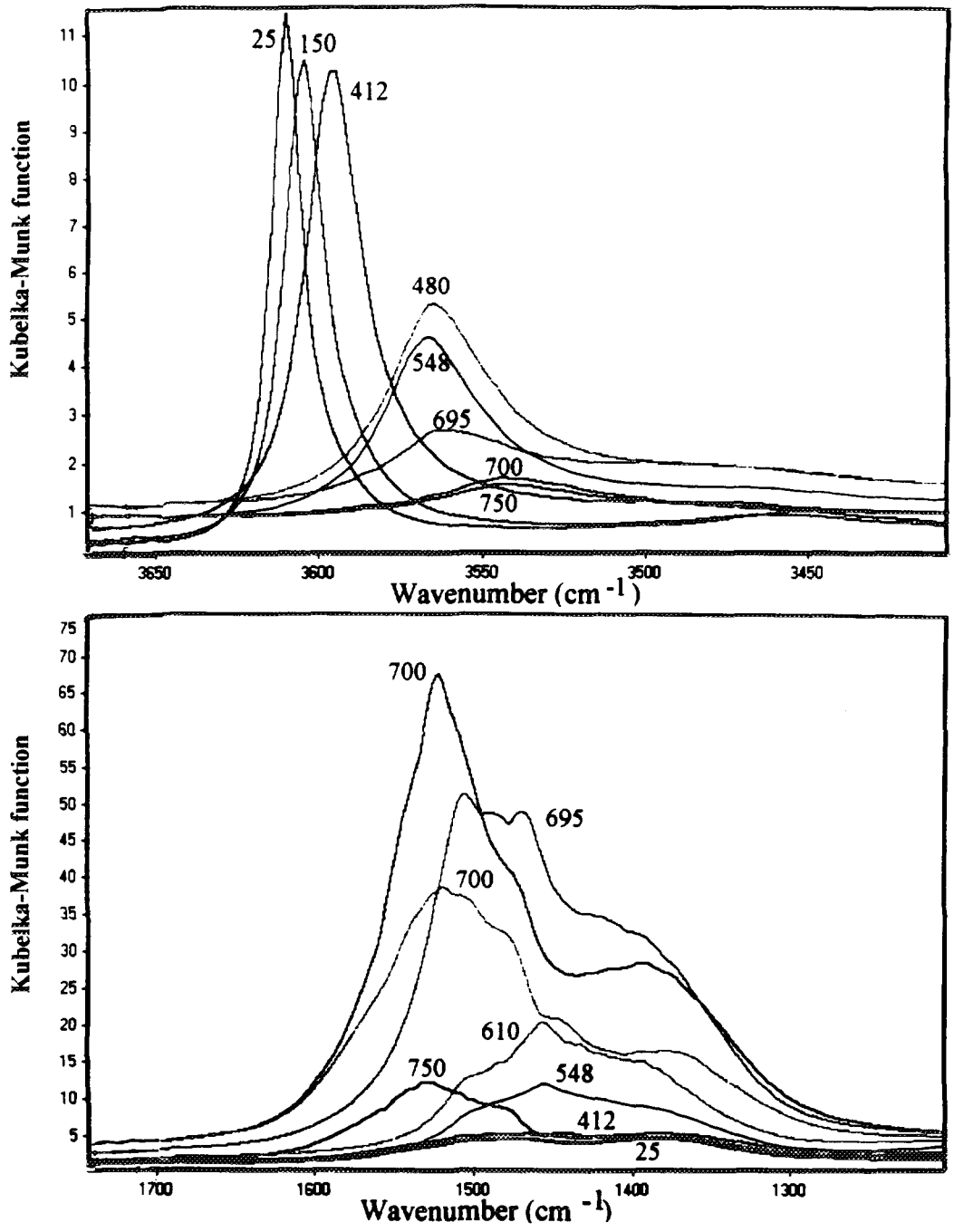

FIG. 3. Diffuse reflectance infrared spectra recorded *in situ* during calcination at the indicated increasing temperatures (expressed in °C).

ture is increased to 750°C several changes are observed in the hydroxyl range: (i) a shift to lower frequency (from 3612 to 3545 cm^{-1}), (ii) a drastic decrease in the intensity of the main hydroxyl band, and (iii) the disappearance of the band at 3450 cm^{-1}. Concerning the carbonate range, the bands characteristic of several carbonate species (identified previously in transmission experiments) first increase with temperature up to around 700°C, with changes in frequency expected from a mixture of different species. At higher temperature, up to 750°C, the carbonate bands decrease dramatically, demonstrating the instability of these species at high temperature. These important changes in the DRIFT spectra during the calcination procedure unambiguously reflect several features: (i) the decomposition of the initial $La(OH)_3$ phase, mostly between 25 and 500°C, (ii) the transient carbonation of the surface,

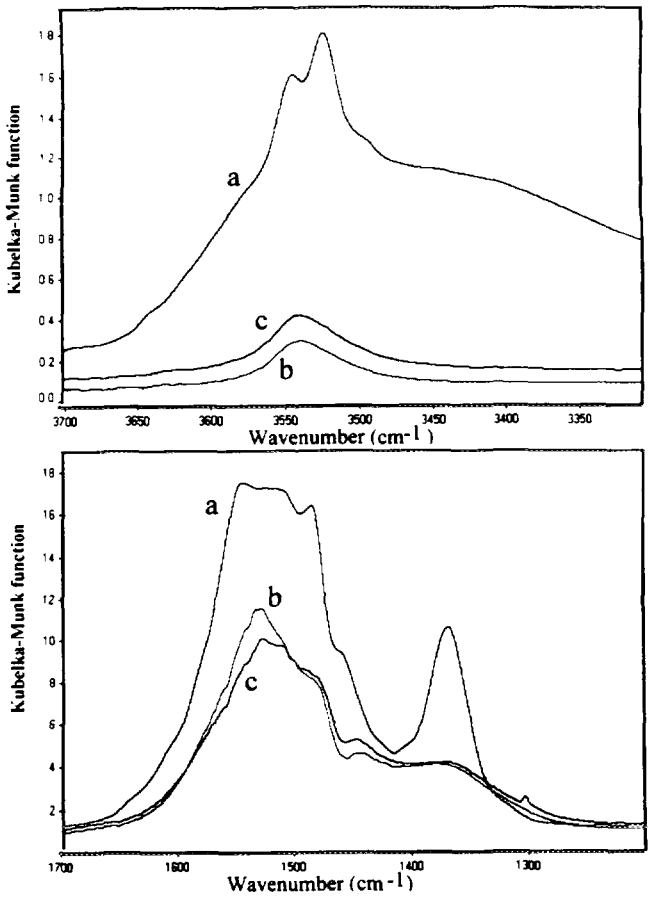

FIG. 4. Diffuse reflectane infrared spectra recorded *in situ* under the indicated conditions: (a) at 25°C after calcination under O_2 at 750°C; (b) at 750°C under O_2; (c) at 750°C under $CH_4/O_2/He$.

between about 500 and 700°C, and (iii) the decomposition of the carbonate and hydroxyl phases at temperatures higher than 700°C. It is thus directly proved that at high temperature (750°C) under flowing oxygen, the lanthana surface is essentially dehydroxylated and decarbonated.

In order to make comparisons with the data obtained at room temperature in transmission mode after calcination at 750°C, a DRIFT spectrum was recorded after the cell cooled to 25°C under flowing oxygen (Fig. 4a). Within the differences expected between transmission (through thin compressed wafer) and diffuse reflectance (through deep powder layer) experiments, similar absorption frequencies are observed: a small band at 3650 cm^{-1} (which corresponds to the band at 3660 cm^{-1} observed in transmission spectra), broad bands between 3550 and 3400 cm^{-1} in the hydroxyl range, and a complex series of bands in the carbonate range. By comparison with the spectra recorded at 750°C under flowing oxygen (Fig. 4b) it is clear that the hydroxyl and carbonate bands have been restored upon the cooling of the calcined sample. This confirms the extreme ability of the lanthana surface to trap any traces of water or carbon dioxide at low temperature.

The effect of the OCM reaction on the surface composition was determined after the $CH_4/O_2/He$ mixture was admitted at 750°C into the DRIFT cell (Fig. 4c). As can be seen by comparing the spectrum in Fig. 4c with the spectrum in Fig. 4b recorded under flowing oxygen, almost no change occurred either for the remaining OH groups or for the residual carbonate species, through the surface was effectively "working," as attested by simultaneous GC analysis. This important feature, never reported in the literature to our knowledge, well emphasizes that under the reaction conditions the catalytic surface remains essentially free from stable adsorbed species such as hydroxyl or carbonate groups. It confirms what was deduced from transmission experiments: any carbonation and hydroxylation of the lanthana surface under the reaction conditions is likely to be mostly transient since it derives directly from fast catalytic cycles; the related intermediate species are therefore not detecable by *in situ* infrared spectroscopy. Let us note, however, that the remaining traces of carbonates observed by *in situ* DRIFT spectroscopy could be related to the traces of bulk oxycarbonates observed elsewhere by *in situ* XRD (16).

Surface composition by X-ray photoelectron spectroscopy. XPS analysis made possible a complementary description of the first layers of the La_{650} catalyst (i.e., at a depth of about 10 nm). XPS spectra (C_{1s} and O_{1s}) are reported in Fig. 5.

The O_{1s} spectra after calcination and after OCM reaction (Figs. 5a and 5c, respectively) present a maximum at 528.8 eV and a large shoulder around 531.3 eV. (The smallest peak at low energy will not be considered since it corresponds to an oxide species of the sample holder, as deduced from a blank experiment.) The former peak at 528.8 eV may be unambiguously assigned to lattice oxygen O^{2-}. The latter corresponds to a range of energy which is characteristic of oxygen atoms belonging to carbonate or hydroxyl groups (15). Due to the poor resolution of the peak, this shoulder around 531.3 eV could therefore be a combination of peaks corresponding to several species of close binding energy.

In the C_{1s} spectra recorded after oxygen treatment (Fig. 5b), besides the carbon peak due to adventitious hydrocarbons at 284.5 eV, another peak is observed at higher energy (around 289 eV), which corresponds typically to a carbon atom belonging to a carbonate group (15). As for oxygen, the smallest peak at low energy will not be considered since it corresponds to adventitious carbon present on the sample holder, as observed in the blank spectrum; note that for the following spectra, a narrower XPS window has been used, avoiding the side signals dealing with the sample holder. From the FTIR observations reported above and in accordance with Taylor and

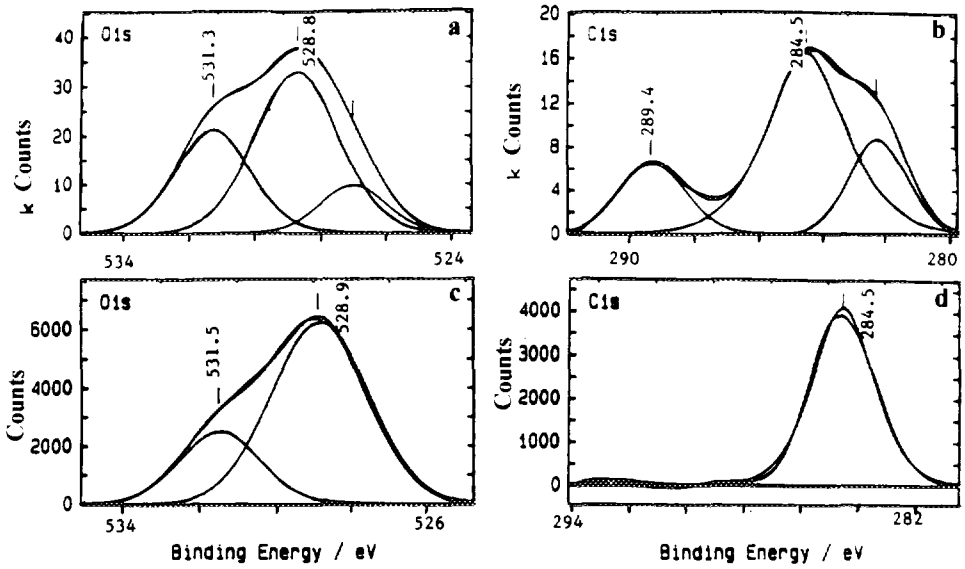

FIG. 5. XPS spectra (smoothed and corrected for background) recorded at room temperature after the indicated treatments: (a), (b) calcination at 650°C; (c), (d) reaction at 750°C.

Schrader (13) and Bernal *et al.* (12), the carbonate group at 289 eV is most probably a dioxomonocarbonate $La_2O_2CO_3$. After reaction at 750°C (Fig. 5d) the peak attributed to carbonates almost disappeared.

On the basis of the above assignments and from the expected C_{1s} to O_{1s} atomic ratios in the carbonate groups, the distribution of the different phases La_2O_3, $La(OH)_3$, and $La_2O_2CO_3$ has tentatively been evaluated (Table 2). Although these values remain semiquantitative due to uncertainty on the deconvolutions and the method, the following points are noteworthy.

(i) Surface hydroxyls are always detected, in accordance with the observation of stable OH groups in any FTIR spectrum (DRIFT or transmission) recorded at room temperature. They are likely to come from a partial rehydroxylation of the lanthana surface in the presence of residual water present in the XPS transfer system.

(ii) A carbonate phase is observed after oxygen treatment at 650°C. This is in perfect agreement with the previous results of DRIFT spectroscopy, indicating that, although no bulk carbonation is observed by XRD, surface carbonates are stabilized at that mild temperature.

(iii) After OCM reaction at 750°C, the surface appears to be almost completely decarbonated. This last feature reinforces the previous conclusion that under the reaction conditions at 750°C, the catalytic surface is mostly in the form of La_2O_3, including only traces of stabilized carbonate or hydroxide phase.

Morphology. TEM micrographs of the reacted La_{750} solid are reported in Fig. 6. The lanthanum oxide essentially consists of tridimensional particles, which are more or less agglomerated (Fig. 6a). Despite a rather wide size distribution, the elementary particles present a mean diameter of about 400 nm. Assuming a simple model of spherical particles, this mean size gives a specific area of 2.5 m^2/g, which effectively corresponds to the BET value of the studied samples. It may be concluded from the above agreement that the reacted catalysts are fully or almost fully crystallized. Actually the particles can be roughly described as polygonal prisms (mostly hexagonal). The height of such prisms is evaluated from the rectangular particles which are assumed to be the side faces of the prism. The shape of these particles enables them to be tightly agglomerated for forming large ensembles. Thickness fringes are visible on some particles, which mean that the polygonal prisms present slanting faces, with truncated tops and bottoms. Structure defects are also identified: (i) grain boundaries of high tension, probably resulting from sintering of the particles (Fig. 6b), (ii) crystalline microareas with different plane orientations

TABLE 2

Percentage of Surface Species Calculated from XPS Data as a Function of Pretreatment Conditions

Treatment	Surface composition (%)		
	La_2O_3	$La_2O_2CO_3$	$La(OH)_3$
O_2 650°C	58	23	19
O_2/CH_4 750°C	73	<1	25

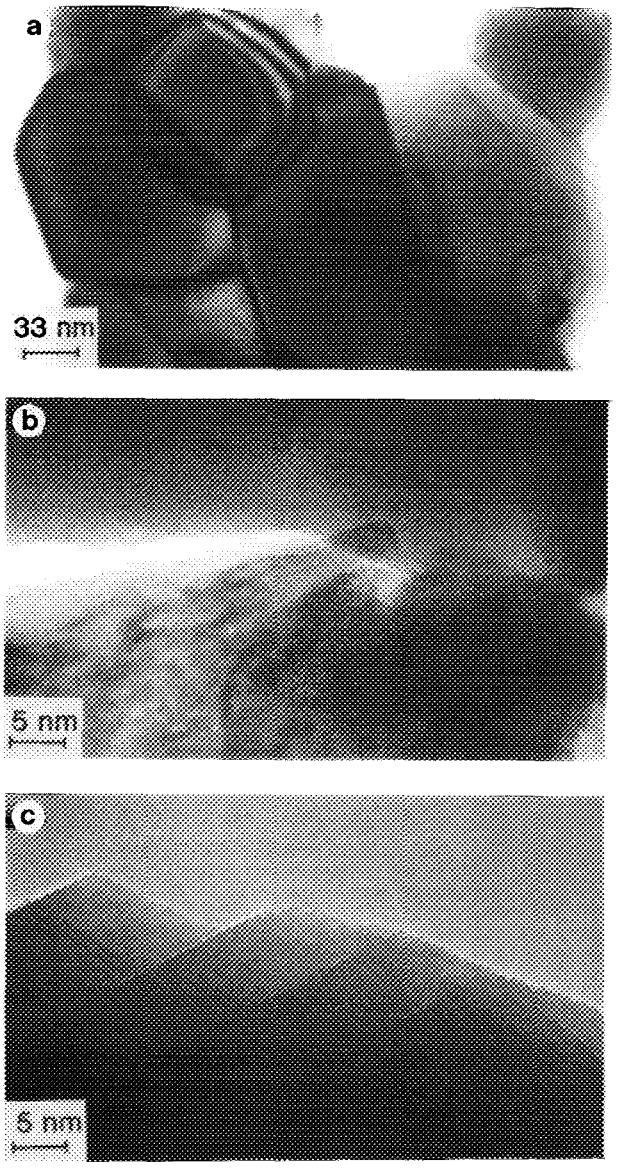

FIG. 6. Transmission electron micrographs after reaction at 750°C.

(Fig. 6b), and (iii) rather regular steps on the outer planes (Fig. 6c). The number of crystalline planes observed on each step can be directly evaluated. Then, assuming that the steps are as high as those sketched in Fig. 7, this leads to an average percentage of step-edge out of total surface atoms between 5 and 10%.

These step-edge atoms obviously present a number of nearest neighbour ions of the opposite sign lower than those for surface and bulk atoms. They can therefore be considered as low-coordinate ions, following Che and Tench (24) in their review of oxide surfaces. They will be referred to later as coordinatively unsaturated sites

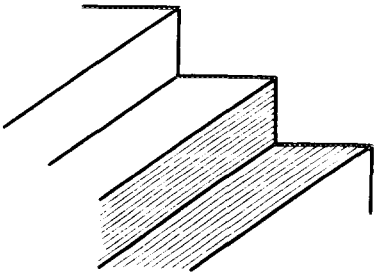

FIG. 7. Sketch of an outer plane of a lanthana particle, allowing one to evaluate the concentration of corner and edge surface atoms.

(CUS). It may be anticipated that these sites, which have been shown to present marked electron donor properties (24), are likely to play a specific role within the process of the OCM reaction.

Though close to the La_{750} ones, the micrographs obtained with the La_{1000} sample show slightly larger particles, in agreement with a lower surface area; in addition the La_{1000} surface is apparently less stepped and smoother than the La_{750} surface.

Particle modelling. From information on the lanthanum oxide after OCM, structural modelling was carried out in order to estimate the dispersion of the oxygen atoms, i.e., the percentage of surface to bulk oxygen atoms. It was based on a simple model assuming bulk La_2O_3 of hexagonal structure (from XRD) and tridimensional particles with the shape and dimensions described in Fig. 8 (from TEM). It must be stressed that this model is an ovesimplification of the actual morphology of the particles, which are polygonal with slanting faces. However, due to the low surface area, it was verified that the oxygen dispersion was little sensitive to the exact shape of the particles.

In the hexagonal unit cell of lanthanum oxide (a = 0.651 nm, c = 0.385 nm), each lanthanum ion is surrounded by 7 oxygen atoms, 4 in tetrahedral coordination $O_{(1)}$ and 3 in octahedral coordination $O_{(2)}$ (Fig. 9). Each of the $O_{(1)}$ and $O_{(2)}$ atoms is bonded to 4 and 6 metal ions, respectively

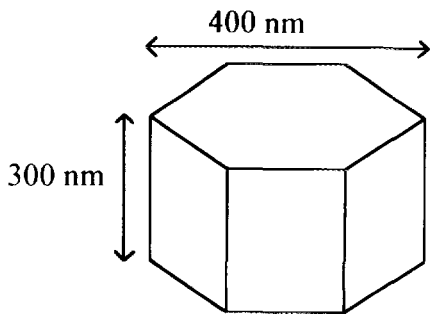

FIG. 8. Sketch of the lanthanum oxide particle used for modelling.

TABLE 3

Structural Characteristics of a Model Lanthana Particle Reacted at 750°C

Atoms	N in the whole particle	N on the surface	Dispersion[a] (%)
La + O	1877	9.0	0.48
La	750	3.0	0.40
O	1127	6.0	0.53
O(1)	750	3.0	0.40
O(2)	377	3.0	0.80

Note. N = number of atoms expressed in million.
[a] Percentage of surface to bulk atoms.

(25). The elementary hexagon is composed of 3 unit cells and contains 6 La atoms, 6 $O_{(1)}$ atoms, and 14 $O_{(2)}$ atoms; n, which represents the number of unit cells at the edge of one face of the hexagon, equals unity in this case. The crystallographic model developed in this work is based on three-dimensional growth of the hexagonal unit cell. It enables one to calculate the number of La, $O_{(1)}$, and $O_{(2)}$ ions present either at the surface of the crystallite or in the whole particle, as a function of the particle size. From the average length of the particles estimated from TEM pictures obtained with the La_{750} sample, the mean lanthana particle would be formed of n = 500 elementary hexagons, which leads to the characteristics reported in Table 3. From these data, it may be emphasized that only around 0.5% of La or O atoms are surface atoms. Using the values of oxygen dispersion (0.53%) and surface area (2.4 m^2/g), the concentration of step-edge surface atoms (CUS) observed by TEM or La_{750} sample is evaluated to be between 1 and 2 $\mu mol/m^2$.

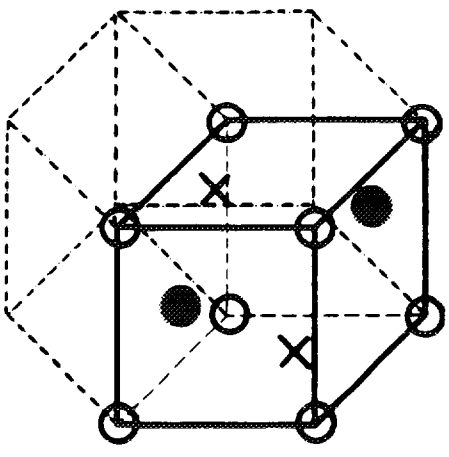

FIG. 9. Elementary hexagonal unit cell of lanthanum oxide. (●) O_1, tetrahedral coordination. (○) O_2, octahedral coordination, X = La.

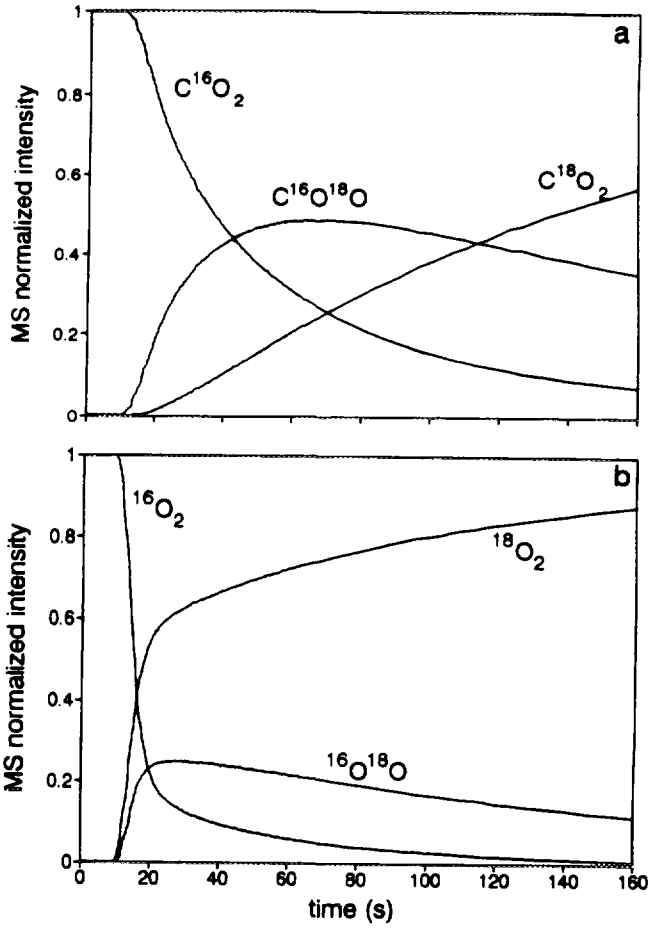

FIG. 10. Normalized carbon dioxide (a) and oxygen (b) transients for an oxygen isotopic switch in the presence of methane ($^{16}O_2/CH_4/He \rightarrow {}^{18}O_2/CH_4/He$) at 750°C. Catalyst loading = 17.3 mg.

Mechanistic Aspects of the Total Oxidation Path

Oxygen labelling. The transient response of carbon dioxide to a $^{16}O_2/^{18}O_2$ switch in the presence of methane (i.e., under OCM conditions) was analyzed in order to determine the origin of the oxygen atoms contained in the produced molecules. Figure 10 reports both the normalized carbon dioxide curves ($C^{16}O_2$, $C^{16}O^{18}O$, and $C^{18}O_2$) and the oxygen curves ($^{16}O_2$, $^{16}O^{18}O$, and $^{18}O_2$) recorded at the reactor outlet, after a $^{16}O_2/^{18}O_2$ switch in the presence of methane on La_{750} catalysts at 750°C. A simple calculation shows that the oxygen atoms of the CO_2 molecules are in statistical equilibrium whatever the considered time within the transient response. The average degree of exchange is equal to 100%. Similar observations were reported by Peil *et al.* on Li/MgO (26). By contrast, the mean degree of exchange for the gaseous oxygen under reaction conditions reaches only 6.5%. The fact that the oxygen isotopic composition of the carbon dioxide is far from the isotopic composition of the gaseous oxygen

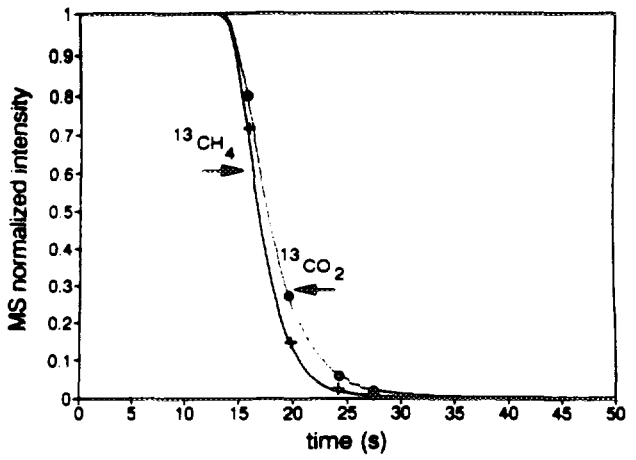

FIG. 11. Normalized carbon transients for a carbon isotopic switch ($^{13}CH_4/O_2/He \rightarrow {}^{12}CH_4/O_2He$) at 750°C. Catalyst loading: 12.6 mg. (—) on-line MS; (---) GC/MS; (+) $^{13}CH_4$, ^{13}CO, $^{13}C_2H_4$, $^{13}C_2H_6$; (○) $^{13}CO_2$.

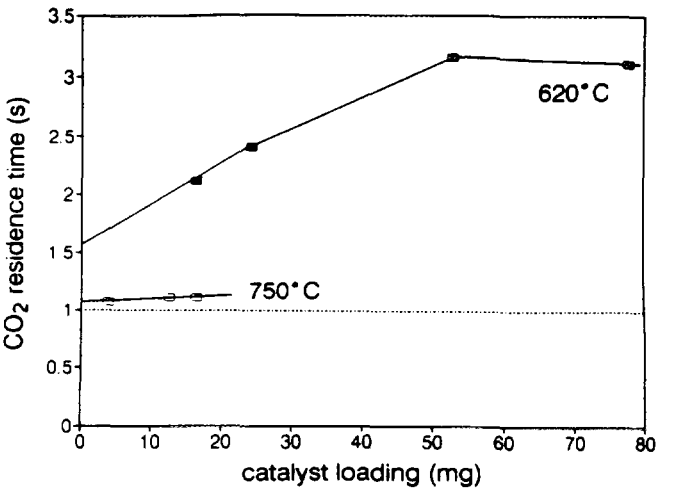

FIG. 12. Mean surface residence time of the CO_2 precursors as a function of catalyst loading and reaction temperature.

excludes any fast gaseous oxidation process leading to CO_2 formation. In this respect, the isotopic scrambling observed for CO_2 indicates that the latter is formed on the surface, from a pool of scrambled ^{16}O and ^{18}O atoms. Furthermore, it is likely that the CO_2 molecules, once formed, undergo several desorption/readsorption processes, which also may account for the statistical mixing of the oxygen atoms.

Carbon labelling. Labelling of the carbon atoms of methane at the reactor inlet was aimed at evaluating the time required for a methane molecule to be transformed into OCM products. Figure 11 reports the normalized isotopic concentration of the carbon-containing molecules after a switch from $^{13}CH_4$ to $^{12}CH_4$ under OCM conditions with the La_{750} sample. The transient responses of C_2H_6, C_2H_4, and CO (labelled and nonlabelled) are quite close to that of CH_4 (within the time resolution of the technique); this confirms that the C_2 hydrocarbons and carbon monoxide are formed via routes involving very short residence times in the catalytic system.

At variance with C_2 and CO, a significant time lag was observed between the CO_2 transients and the reference signal (inert gas or methane over empty reactor). Integrating this delay provided the mean residence time of carbon dioxide in the system. As pointed out under Experimental, this overall time includes both the catalytic residence time of a CO_2 precursor on the catalytic site and the noncatalytic residence times due to readsorption/desorption equilibria of CO_2 along the catalytic bed and in the gas line. The chromatographic effect occurring along the catalyst bed was corrected for by extrapolating the overall residence time to zero loading. The chromatographic effect related to the gas line was evaluated as 1.0 s by using prereactors (see Experimental) (Fig. 12).

The true residence times of CO_2 precursors determined for the La_{750} and La_{1000} samples are reported in Table 4. Qualitatively, the fact that residence times of CO_2 precursors are measurable, at variance with the other OCM products, strongly supports the idea that carbon dioxide is formed through a series of slow surface steps.

In a simplified way the quasi-exponential CO_2 transient (Fig. 11) was modelled according to the following pseudo-first-order rate equation (9, 27)

$$r_{CO_2} = k \text{ (concentration of oxidation sites)}, \quad [3]$$

where r_{CO_2} is the rate of CO_2 formation measured under steady-state conditions and k is a pseudo-rate constant, i.e., the reverse value of the mean residence time τ of a CO_2 precursor on an active site. This formalism assumes that the rate-determining step involves mostly the oxidation of a surface precursor (generated from the methane activation); it possibly includes several elementary steps

TABLE 4

Intrinsic Data (Mean Residence Time, Site Reactivity, Reaction Rate, and Site Concentration) for the Total Oxidation Pathway (Leading to CO_2)

Sample	T (°C)	Residence time τ (s)	Site reactivity k (s^{-1})	r_{CO_2} ($\mu mol/m^2 \cdot s$)	Concentration of oxidation sites ($\mu mol/m^2$)
La_{750}	620	0.6	1.7	1.4	0.81 ± 0.02
	750	0.1	10.0	7.2	0.72 ± 0.02
La_{1000}	620	<0.2	>5	1.5	<0.3
	750	<0.05	>20	8.2	<0.4

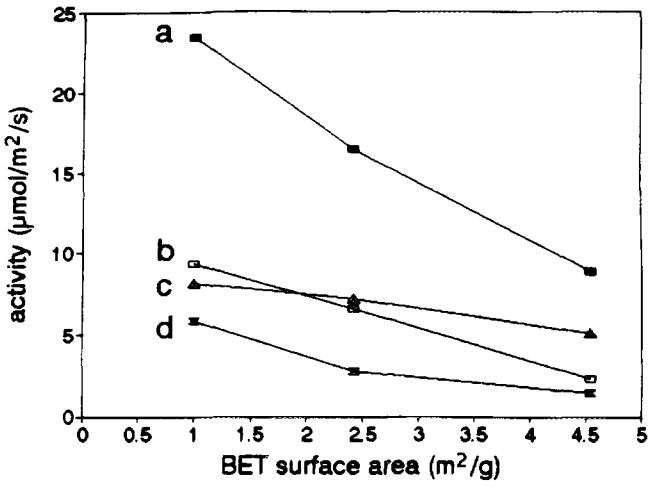

FIG. 13. Changes in the intrinsic rates of (a) methane conversion, (b) C_2, (c) CO_2, and (d) CO formation as a function of the BET surface area.

lumped together, involving gaseous or adsorbed oxygen. The kinetic contribution of the oxygen activation in each of these oxidation steps would be included in the overall pseudo-rate constant k. This assumption seems reasonable if one considers the low value obtained for the kinetic isotopic effect on CO2 in earlier work (8). From the experimental measurement of r_{CO_2} and τ, the concentration of oxidation sites can therefore be estimated from Eq. [3] (Table 4). The interesting point is that within the uncertainty of the method, the concentration of the total oxidation sites for a given catalyst remains independent of the reaction temperature, as expected from a stabilized catalyst; only their reactivity increases with temperature. The dependence on surface area is described in the next paragraph.

Dependence of intrinsic kinetic data and catalytic performance on surface area. Figure 13 reports the changes in specific rates of methane conversion and C_2, CO, and CO_2 formation at 750°C as a function of the BET surface area. As can be seen, the intrinsic activities tend to decrease with increasing surface area, along with the selectivity towards C_2 hydrocarbons. The latter result was already indicated as a general trend observed for the OCM reaction whatever the type of catalyst (28).

If one compares in Table 4 the intrinsic kinetic data obtained for different samples, it is noteworthy that decreasing the surface area tends to decrease the intrinsic concentration of total oxidation sites and to increase their reactivity.

DISCUSSION

The information obtained in the present study of lanthanum oxide phases under OCM reaction conditions may be discussed separately as follows.

Catalyst Structure

Mostly La_2O_3 material of hexagonal structure (XRD) is retained when the reaction is carried out at 750°C. From TEM pictures, elementary particles of La_2O_3 appear as polygonal (often hexagonal) prisms, with slanting faces truncated at the top and bottom. These particles tend to sinter during thermal treatment, which would account for the observed decrease in BET surface area with increasing the calcination temperature. Local surface defects are detected on the micrographs: grain boundaries, crystalline microareas; and regular steps on the sides of the particles. The concentration of the atoms located at the edge of these steps, considered as coordinatively unsaturated sites (CUS), has been evaluated to be 5–10% of the surface atoms. On the basis of a simple model proposed for the lanthana particles, this concentration would lead to an absolute number of CUS of 10^{-6}–2×10^{-6} mol/m^2.

State of the Working Surface

At 750°C, under OCM conditions, the "working" La_2O_3 surface is essentially decarbonated and dehydroxylated (*in situ* DRIFT) and only transient intermediates related to the catalytic cycles producing CO_2 and H_2O are likely to maintain residual surface carbonates and hydroxyl groups. From the comparison between *in situ* IR analyses and *ex situ* XPS or transmission IR analyses achieved at room temperature after high temperature treatment, it may be emphasized that the large amounts of hydroxyl and carbonate groups detected by the latter techniques result from the trapping of water and carbon dioxide on the surface when the sample is cooled.

Nature of the Active Sites

For the case of the La_{750} sample on which most of the characterization study was focused, specific and localized hydroxyl groups (La–OH terminal species) detected at room temperature are evolved as H_2O at reaction temperature (FTIR). This surface dehydroxylation process is likely to generate pair sites such as {O^{2-}, vacancy} which could be involved in the formation of methoxide ions leading to CO_x products within the OCM process. A plausible assumption is to relate these sites coming from the dehydroxylation of specific terminal La–OH groups to the CUS sites observed and numbered by electron microscopy and particle modelling.

From a quantitative point of view, the concentration of total oxidation sites was directly evaluated from the transient kinetics (around 0.8×10^{-6} mol/m^2). It is of the utmost interest that this amount is quite close to the concentration of coordinatively unsaturated oxygen atoms (O_{CUS}) (between 10^{-6} and 2×10^{-6} mol/m^2) determined by TEM and particle modelling. This correlation, to our knowledge, as yet never reported, tends to

demonstrate that the total oxidation of methane proceeds preferentially on very localized sites, characterized by a high degree of unsaturation.

By atomistic computer simulation techniques, Ilett and Islam (29) have recently indicated a clear differentiation between the tetrahedral $O_{(1)}$ and octahedral $O_{(2)}$ types of lattice oxygen, the former being in a more favourable position to form vacancies, able to migrate and create holes on a neighbouring $O_{(2)}$ position. From that statement, it may be speculated further that the pair site we propose for total oxidation would associate a weakly coordinated lattice $O_{(2)}$ oxygen to an $O_{(1)}$ oxygen vacancy.

A plausible oxidation process can be proposed on the basis of the above observations and from the previous conclusions of IR analysis: a reaction between gaseous $CH_3\cdot$ radicals and coordinatively unsaturated surface oxygen leading to $O\text{–}CH_3^-$ methoxide ions, followed by a sequence of surface oxidation steps leading to CO_3^{2-} groups, in equilibrium with the gaseous CO_2, as indicated in Eqs. [4]–[7]:

$$CH_3\cdot + \{O^{2-}_{CUS} + \square\} \rightarrow O\text{–}CH_3^- + \boxdot \quad [4]$$

$$O\text{–}CH_3^- + 4O^- \rightarrow CO_3^{2-} + OH^- + H_2O + 2\boxdot \quad [5]$$

$$CO_3^{2-} \Leftrightarrow CO_2 + O^{2-}_{CUS} \quad [6]$$

$$2\,OH^- \rightarrow H_2O + O^{2-} + \square. \quad [7]$$

Structure Sensitivity

Following the conclusion that the total oxidation pathway involves specific sites related to the catalyst structure, it may be anticipated that the CO_2 selectivity must be highly sensitive to the structure of the catalyst, most probably in relation to its surface area, as observed on MgO by Hargreaves *et al.* (30) and on La_2O_3 catalysts by Le Van *et al.* (14). Several assumptions, eventually contradictory, were proposed to account for this structure sensitivity, such as the active and selective role of either low-index planes (14) or high-index planes (30); surface defects, such as grain boundaries, possibly developed after alkali promotion (30), were also considered as possible structural factors for the reaction orientation.

In the present study, it has clearly been established that within a La_2O_3 series, the lower the surface area, the higher the intrinsic activity and the C_2 selectivity (Fig. 13).

Concerning the intrinsic activity, it was initially proposed by Lunsford and his co-workers (31) and recently confirmed by our group by means of isotopic transient experiments carried out on a TAP reactor (11), that the active sites able to activate methane are oxygen species O^- (or O_2^{2-}) resulting from the activation of molecular oxygen on lattice O^{2-} atoms and oxygen vacancies $\square$, following

$$\tfrac{1}{2}\,O_2 + \{O^{2-} + \square\} \Leftrightarrow 2\,O^-. \quad [8]$$

The low surface area samples were shown to result from particle agglomeration favouring grain boundaries and therefore lattice vacancies, in agreement with Hargreaves *et al.* (30). Accordingly, it is proposed that the high intrinsic activity observed for these low surface area samples results from an enhanced oxygen activation due to a high concentration of lattice vacancies, possibly arising from $O_{(1)}$ positions, following Ref. (29).

Concerning the total oxidation pathway, it has been shown in the present study that low surface area samples exhibit an intrinsic concentration of "toxic" step sites (CUS) lower than high surface area samples, which may be related to a smoothing effect of the particle sintering. We propose to correlate the low concentration of total oxidation sites to the beneficial effect on C_2 selectivity observed on sintered solids.

In order to support the above conclusions, recent experiments were carried out aimed at poisoning selectively the toxic sites of the lanthana surface. It was shown that a controlled addition of sulfate anions decreases the CO_2 selectivity without much affecting the methane conversion. In addition, XPS data tend to indicate that the surface anions are specifically located on defect zones of the lanthana particles (32). These results considerably strengthen the above explanation of the OCM structure sensitivity.

CONCLUSION

The present work provides strong indication that several types of active sites are involved in the oxidative coupling of methane over lanthana catalysts: (i) basic sites associated with oxygen vacancies for dissociating gaseous oxygen into atomic species able to activate methane molecules; and (ii) localized low-coordinate atoms on which methyl radicals would react to be further oxidized into CO_2. Structure and morphology effects on intrinsic catalytic performances, explained within the above statement of differentiated sites, tend to indicate that large surface areas are rather detrimental for C_2 selectivity. In addition, it may be questioned whether any kinetic approach based on classical Langmuir assumptions of site uniformity remains valid for an oxide surface as described in the present study.

ACKNOWLEDGMENTS

This work was supported by the European Community (Joule Programme–Contract JOUF 0044-C). Thanks are due to Drs. G. A. Martin,

M. Brun, P. Delichère, and C. Leclercq for valuable technical assistance and helpful discussions.

REFERENCES

1. Keller, G. E., and Bhasin, M., *J. Catal.* **73,** 9 (1982).
2. Lunsford, J. H., *in* "Methane Conversion by Oxidative Coupling" (E. E. Wolf, Ed.) p. 3. Van Nostrand–Reinhold, New York, 1992.
3. Feng, Y., Niiranen, J., and Gutman, D., *J. Phys. Chem.* **95,** 6558 and 6564 (1991).
4. Buyevskaya, O. V., Rothaemel, M., Zanthoff, H. W., and Baerns, M., *J. Catal.* **146,** 346 (1994).
5. Ito, T., Watanabe, T., Tashiro, T., and Toi, K., *J. Chem. Soc. Faraday Trans.* **85,** 2381 (1989); Ito, T., Tashiro, T., Watanabe, T., Toi, K., and Kobayashi, H., *J. Phys. Chem.* **95,** 4476 (1991).
6. Shi, C., Hatano, M., and Lunsford, J. H., *Catal. Today* **13,** 191 (1992).
7. Lehmann, L., and Baerns, M., *Catal. Today* **13,** 265 (1992).
8. Lacombe, S., Sanchez M., J. G., Delichère, P., Mozzanega, H., Tatibouët, J. M., and Mirodatos, C., *Catal. Today* **13,** 273 (1992).
9. Mirodatos, C., *Catal. Today* **9,** 83 (1991).
10. Gleaves, J. T., Ebner, J. R., and Kuechler, T. C., *Catal. Rev. Sci. Eng.* **30,** 49 (1988).
11. Lacombe, S., Zanthoff, H. W., Mirodatos, C., submitted for publication.
12. Bernal, S., Diaz, J. A., Garcia, R., and Rodriguez-Izquierdo, J. M., *J. Mater. Sci.* **20,** 537 (1985).
13. Taylor, R. P., and Schrader, G. L., *Ind. Eng. Res.* **30,** 1016 (1991).
14. Le Van, T., Che, M., Kermarec, M., Louis, C., and Tatibouët, J. M., *Catal. Lett.* **6,** 395 (1990).
15. Briggs, D., and Seah, M. P., *in* "Practical Surface Analysis, Auger and X-ray Photoelectron Spectroscopy" John Wiley & Sons, Chichester, 1990.
16. Squire, G. D., Luc, H., and Puxley, D. C., *Appl. Catal.* **108,** 261 (1994).
17. Rosynek, M. P., and Magnuson, D. T., *J. Catal.* **46,** 402 (1977); **48,** 417 (1977).
18. Hair, M. L., *in* "Infrared Spectroscopy in Surface Chemistry" Dekker, New York, 1967.
19. Turcotte, R. P., Sawyer, J. O., and Eyring, L., *Inorg. Chem.* **8,** 238 (1969).
20. Le Van, T., Che, M., Tatibouët, J. M., and Kermarec, M., *J. Catal.* **142,** 18 (1993).
21. Lehmann, L., and Baerns, M., *J. Catal.* **135**(2), 467 (1992); Nelson, P. F., Lukey, C. A., and Cant, N. W., *J. Catal.* **120,** 216 (1989).
22. Fail, F. S., van Ommen, J. G., and Ross, J. R. H., *Langmuir* **3,** 668 (1987).
23. Tong, Y., and Lunsford, J. H., *J. Am. Chem. Soc.* **113,** 4741 (1991).
24. Che, M., and Tench, A. J., *Adv. Catal.* **31,** 77 (1982).
25. Hyde, B. G., and Andersson, S., *in* "Inorganic Crystal Structures," Wiley, New York, 1989.
26. Peil, K. P., Goodwin, Jr., J. G., and Marcelin, G., *J. Phys. Chem.* **93,** 5977 (1989): *J. Catal.* **131,** 143 (1991).
27. Mirodatos, C., Holmen, A., Mariscal, R., Martin, G. A., *Catal. Today* **6,** 601 (1990).
28. Martin, G. A., Mirodatos, C., *in* "Methane Conversion by Oxidative Coupling" (E. E. Wolf, Ed.) p. 351. Van Nostrand–Reinhold, New York, 1992.
29. Ilett, J., and Islam, M. S., *J. Chem. Soc. Faraday Trans.* **89,** 3833 (1993).
30. Hargreaves, J. S. J., Hutchings, G. J., and Joyner, R. W., *Catal. Today* **6,** 481 (1990); **10,** 259 (1991).
31. Driscoll, D. J., Martir, W. Wang, J.-X., and Lunsford, J. H., *J. Am. Chem. Soc.* **107,** 58 (1985); Lin, C. H., Campbell, J. X., Wang, J. X., and Lunsford, J. H., *J. Phys. Chem.* **90,** 534 (1986).
32. Borges, H., Lacombe, S., and Mirodatos, C., *Catalysis Today* **21,** 289 (1994).